

Rich Club Analysis of Structural Brain Connectivity at 7 Tesla versus 3 Tesla

Emily L. Dennis¹, Liang Zhan¹, Neda Jahanshad¹, Bryon A. Mueller², Yan Jin¹,
Christophe Lenglet³, Essa Yacoub³, Guillermo Sapiro⁴, Kamil Ugurbil³, Noam Harel,
Arthur W. Toga¹, Kelvin O. Lim², Paul M. Thompson¹

¹Imaging Genetics Center, Laboratory of Neuro Imaging, UCLA, Los Angeles, CA

²Department of Psychiatry, University of Minn., Minneapolis, MN

³Center for Magnetic Resonance Research, University of Minn., Minneapolis, MN

⁴Department of Electrical and Computer Engineering, Duke University, Durham, NC

Abstract

The ‘rich club’ is a relatively new concept in brain connectivity analysis, which identifies a core of densely interconnected high-degree nodes. Establishing normative measures for rich club organization is vital, as is understanding how scanning parameters affect it. We compared the rich club organization in 23 subjects scanned at both 7 and 3 Tesla, with 128-gradient high angular resolution diffusion imaging (HARDI). The rich club coefficient (RCC) did not differ significantly between low and high field scans, but the field strength did affect which nodes were included in the rich club. We also examined 3 subjects with Alzheimer’s disease and 3 healthy elderly controls to see how field strength affected the statistical comparison. RCC did not differ with field strength, but again, which nodes differed between groups did. These results illustrate how one key parameter, scanner field strength, impacts rich club organization - a promising concept in brain connectomics research.

1 Introduction

The ‘rich club’ is an emerging concept in the graph theoretical analysis of brain networks. Initially described in [1], it was first applied to brain networks in [2]. In graph-based analyses of brain connectivity, brain regions are represented as nodes and a set of edges represent the connections between them. These connections may be defined based on fiber tracts extracted from diffusion MRI, or based on time-course correlations between different brain regions in functional MRI data. For brain networks, the rich club is defined as a central core of high-degree nodes that are more highly interconnected than would be expected simply from their high degree. Some authors argue that the rich club is crucial for understanding global network efficiency; an attack on rich club nodes disproportionately affects global efficiency [2]. Rich club connectivity organization changes with age as brain connectivity strengthens [3]. Brain networks are complex, and the rich club concept offers a principled approach for dimension reduction: it identifies a key set of crucial nodes that contribute maximally to network

efficiency. The *rich club coefficient*, $\phi(k)$, represents the density of connections between the rich club nodes according to the following equation:

$$\text{Eq. 1 } \phi(k) = \frac{E_{>k}}{N_{>k}(N_{>k}-1)}$$

Here k is the degree of the nodes, $E_{>k}$ is the number of links between nodes with degree k or greater, and $N_{>k}$ is the total number of possible connections if those nodes of degree k were fully connected. Van den Heuvel and Sporns also introduced $\phi_{norm}(k)$, which is $\phi(k)$ divided by the rich club coefficient calculated in a series of random networks ($\phi_{random}(k)$) of the same size with a similar distribution of edges [2]. A $\phi_{norm}(k)$ value > 1 indicates rich-club organization in the network.

The rich club, as it pertains to brain networks, is a new topic of interest, and little is known about its stability across MRI scanning parameters. If network parameters depend on the scanner field strength or other imaging parameters, researchers need to be aware of this, to ease pooling of multi-site data and resolve apparent discrepancies among studies. We hypothesized that the brain's fiber network could be imaged reproducibly at 7 and 3 Tesla to yield the same rich club content and coefficient, despite differences in scanning protocols (high-field versus standard magnetic field strength). We set out to examine how MR field strength affects rich club properties in 23 young adults scanned at both 7 and 3 T. In pilot work, we also examined 3 subjects with Alzheimer's disease (AD) and 3 age- and sex-matched healthy controls (HC) to see how statistical comparisons might be affected by field strength. These data come from prior work by our group examining how MR field strength affects connectivity, including more basic tractography measures [4].

2 Methods

2.1 Subject demographic and image acquisition

Whole brain anatomical and DW-MRIs at both 7 and 3 T were collected from 23 young adults (11 female, mean age=23.8, SD=2.6) and 6 elderly subjects (3 AD: 2 female, mean age=76.1, SD=3.2; 3 HC: 2 female, mean age=78.3, SD=2.4); the protocols are detailed in [5,6]. Standard head coils were used on both systems: the 12-channel receive-only array on the 3T, and a Nova 24 channel transmit/receive coil on the 7T. The reconstruction method for the 3T scanner was adaptive recombine (AC), while the default multi-channel reconstruction method for the DWI data on the 7T scanner was sum-of-squares (SOS). 3T DW-images were acquired with the following acquisition parameters: GRAPPA mode; acceleration factor PE=2; TR/TE=7800/82 ms; FOV=192x192 mm, isotropic voxel size=2 mm. 143 images were collected per subject: 15 b_0 and 128 diffusion-weighted ($b=1000$ s/mm²). 7T DW-images were acquired with the following acquisition parameters: GRAPPA mode; acceleration factor, PE=2; TR/TE=5700/57 ms; FOV=256x256 mm, isotropic voxel size=2 mm. 143 images were collected per subject: 15 b_0 and 128 diffusion-weighted ($b=1000$ s/mm²). T1-weighted anatomical images were acquired at 3 Tesla with the following acquisition parameters: GRAPPA mode; acceleration factor PE=2; T1/TR/TE=1100/2530/3.65 ms; echo spacing = 8.5 ms; flip angle = 7°; slice thickness = 1.0 mm, with an acquisition matrix of 256x256. All subjects gave informed consent

after study protocols were explained.

2.2 Image preprocessing and registration

All DWI data were visually inspected by an experienced rater for evidence of the known Siemens vibration dropout artifact [7]. No dropout artifact was found in the DW data. All raw DWI images were corrected for distortions due to eddy currents and motion using the *eddy_correct* function from the FSL toolbox (<http://fsl.fmrib.ox.ac.uk/fsl>) [8,9]. Geometric distortions due to magnetic susceptibility were then corrected using a field map collected just before the DTI, using the FSL *prelude and fugue* functions. Non-brain regions were removed from a T2-weighted image (b_0) in the corrected DWI dataset using the *bet* function in FSL. A trained neuroanatomical expert manually edited the T2-weighted scans to refine the brain extraction and to ensure the same brain coverage among different protocols. This step was important to avoid bias, as different connectivity patterns might be recovered if brain coverage varies. All analyses below are based on this preprocessed dataset.

2.3 Brain connectivity computation

Tractography and cortical networks were computed in the native space of the data. The Diffusion Toolkit (<http://trackvis.org/dtk/>, [10]) uses these parameters to generate 3D fiber tracts, using the Orientation Distribution Function model, computed using the 2nd order Runge-Kutta method [11]. We used all voxels (with $FA \geq 0.2$) as seed voxels to generate the fibers. Paths were stopped when they reached a region with $FA < 0.2$; they were also stopped if the fiber direction encountered a sharp turn (critical angle threshold $\geq 30^\circ$). After tractography, a spline filter was applied to each generated fiber, with units expressed in terms of the minimum voxel size of the dataset (2 mm). Each subject's dataset contained 25,000-40,000 useable fibers (3D curves). Duplicate fibers and very short fibers ($< 10\text{mm}$) were removed. Although we did not do this here, some researchers normalize fiber count by ROI volume at this point [12].

Cortical and subcortical ROIs were defined using the Harvard Oxford Cortical and Subcortical probabilistic atlases [13]. Midline cortical masks were bisected into left and right components, to define separate hemispheric ROIs for each cortical region. Since this is a probabilistic atlas, the masks were set to a liberal threshold of 10% to include tissue along the gray-white matter interface, where fiber orientation mapping and tractography are most reliable [14]. To register these ROIs to each subject's DTI space, we used FSL's *flirt* function to determine the optimal affine transformation between the MNI152 T1 average brain (in which the Harvard Oxford probabilistic atlases are based) and each subject's unique FA image. We used a 12 degree-of-freedom registration with a mutual information cost function. We applied the resulting transformation to register the 110 ROIs to each subject's DTI space using nearest neighbor interpolation. To ensure that ROI masks did not overlap with each other after registration, each voxel was uniquely assigned to the mask for which it had the highest probability of membership. For a list of ROIs, see [4]. We did not include the brainstem and cerebellum ROIs, giving us a total of 110 ROIs.

For each pair of ROIs, the number of detected fibers connecting them was determined from the tractography results. A fiber was considered to connect two ROIs if it intersected both ROIs. This process was repeated for all pairs, resulting in an 110x110

matrix. This matrix is symmetric and has a zero diagonal (no self-connections).

2.4 Rich club analyses

On these 110x110 matrices, we used the Brain Connectivity Toolbox ([15]; <https://sites.google.com/a/brain-connectivity-toolbox.net/bct/> Home) to compute the rich club coefficient ($\phi(k)$). We calculated the $\phi(k)$ over values of k (the degree of the nodes) ranging from 0-110 to capture all possible values. To generate the normalized rich club coefficient ($\phi_{norm}(k)$), we simulated 50 random networks. These matrices were first binarized so the actual weights of the edges were not factored in, simply the number of connections. Analyses comparing $\phi(k)$ and $\phi_{norm}(k)$ were performed across all subjects. In order to compare rich club organization, we constructed average graphs for the 3T and 7T datasets. For the young cohort, these were averaged across all 23 subjects, and the group-averaged matrices were thresholded to include only connections found in at least 75% of subjects; this step is helpful to suppress false positive fibers arising from tractography errors. For the elderly cohort, these were averaged separately for the AD and HC subjects. Given the small sample size, we did not threshold the group-averaged matrices. To determine the k cut-off for rich club membership, we used the same criteria as [2]: we included nodes having a degree at least one standard deviation above the average degree. For the young cohort, the average degree for the 3T group-averaged network was 57.4, while for the 7T network it was 54.7. This was not a significant difference, however. This resulted in a k cutoff of 69 at 7T and 71 at 3T, and we used these thresholds for **Figure 1**. We will call these ‘analogous k -levels’ from here on in the paper. For the elderly cohort, the average degree for the 3T AD group-averaged network was 93.5, and in HC it was 91.2; this group difference was significant ($p=0.025$). For the 7T group-averaged networks, the average degree for AD was 73.0, and in HC it was 79.9, a difference that was also significant ($p=2.1 \times 10^{-16}$). These averages are higher than for the young cohort because we could not filter these networks in the same way, given the small sample size.

3 Results

3.1 Rich club coefficient ($\phi(k)$ and $\phi_{norm}(k)$)

We ran a paired-sample t -test at each k -level (the nodal degree threshold) to look for protocol effects on our subjects’ connectomes, by studying both $\phi(k)$ and $\phi_{norm}(k)$ across subjects. We did not detect any significant differences in rich club coefficient, either $\phi(k)$ or $\phi_{norm}(k)$, between protocols in the young cohort. We also did not detect any differences in $\phi(k)$ or $\phi_{norm}(k)$ between AD and HC at 3T or 7T, although admittedly we were underpowered to pick up group differences.

3.2 Rich club organization – Young cohort results

When $k=69$ for 7T and $k=71$ for 3T, as justified above, there were differences in the rich club organization of the group-averaged 3T and 7T matrices. These mostly resulted from the fact that the 3T rich club at $k=71$ included 21 nodes, while the 7T rich club at $k=69$ included only 19 nodes. This was due to a slight difference in average degree, as mentioned above. These results are shown in **Figure 1**.

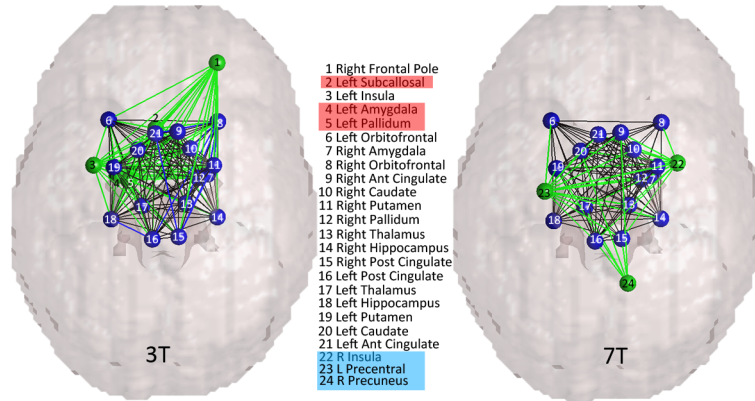


Figure 1. Differences in rich club organization between 3T and 7T scanning protocols. Green nodes are unique to one rich club, blue are common to both. Black edges are common to both rich clubs, blue edges are unique to one rich club but among common nodes, green edges are unique to one rich club due to the unique nodes. 3T k -level=71, 7T k -level=69. The red highlighted nodes are unique to the 3T rich club when N_{node} was kept constant at 19, instead of k -level, blue highlighted nodes are unique to the 7T rich club in the N_{node} analysis.

Knowing that a difference in degree impacted rich club membership, we also compared rich club organization when the *number* of nodes was held constant, rather than looking analogous k -levels, as before. When the node-number (symbolized here by N_{node}) was held constant at 19 nodes, there were still differences in rich club membership. When held constant at $N_{\text{node}}=19$, the common nodes between the two connectomes were nodes 6-21, as listed in **Figure 1**. Those unique to the 7T rich club were nodes 22-24, highlighted in blue, while those unique to the 3T rich club were nodes 2, 4, and 5, highlighted in red. Interestingly, those unique to the 3T rich club are all subcortical, while those unique to the 7T rich club, when $N_{\text{node}}=19$, are all cortical. Following up on this N_{node} analysis, we compared $\phi(k)$ when node number was held constant. **Table 1** shows these results, across a range of N_{node} tested. To do this, we looked at the number of nodes present at k -levels 69-75 for 7T, and then found where this N_{node} boundary was in the 3T network. The N_{node} comparisons are not exact between 3T and 7T, as that would require arbitrarily cutting off nodes that had the same k -level. As we were comparing $\phi(k)$, which is still calculated based on level, arbitrarily cutting off nodes would make comparing the $\phi(k)$ values invalid. This kind of analysis is intended to give a clearer idea of the relationship between the $\phi(k)$ of the 3T and 7T connectomes when the number of nodes is held constant. As seen in **Table 1**, $\phi(k)$ is significantly greater in the 3T connectome across most of this range. We chose to look at a range beginning with 7T k -level=69, as that was the ‘high degree’ threshold for 7T mentioned above, and ending with the last k -threshold at which rich club organization was detectable (75 for 7T, 77 for 3T). We ran a paired-sample t -test on the distribution of $\phi(k)$ at a given k -level between protocols, and used the false discovery rate method (FDR) to correct for multiple comparisons ($q < 0.05$, [16]).

Table 1. Comparison of high-field and standard field protocols maintaining N_{node} . Across a range, $\phi(k)$ was averaged across all subjects. N_{node} indicates the number of nodes at a given k -level. P denotes the p value for a two-tailed t -test comparing the means of the $\phi(k)$ for the 3T and 7T protocols at a given k -level. All results are corrected for multiple comparisons, with the FDR method ($q < 0.05$).

7T k level	69	70	71	72	73	74	75
N_{node}	19	14	14	11	10	9	8
Avg. $\phi(k)$	0.9217	0.9332	0.9434	0.9529	0.9603	0.9674	0.9732
3T k level	72	74	74	75	75	76	77
N_{node}	19	15	15	11	11	9	9
Avg. $\phi(k)$	0.947	0.9577	0.9577	0.9652	0.9652	0.9712	0.9758
p	0.0014	0.0039	0.066	0.073	0.47	0.55	0.64

3.3 Rich club organization – AD/HC comparison

We compared which nodes were included at the statistically determined k cut-offs for rich club membership (3T AD=104, 3T HC=105; 7T AD=90, 7T HC=96). We expected to find differences between the AD and HC subjects, but were most interested in how the differences between groups varied with field strength. Given our small sample size (3 AD, 3 HC), these results are preliminary. These are summarized in **Figure 2**. There were many differences that were only detectable at 3T. Both groups had larger rich clubs at 3T, like the young cohort, again due to lower degree at 7T.

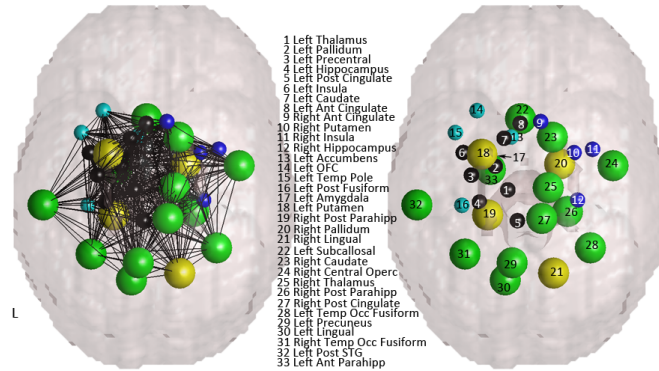


Figure 2. Differences in the comparison of AD versus HC subjects between 3T and 7T scanning protocols. Left image shows rich club nodes with connections, as averaged across all subjects (thresholded to include connections found in at least 66% of subjects), right image shows just the nodes, for clarity. Small nodes showed no effect of field strength, large nodes showed an effect of field strength; black nodes both groups had; blue nodes present in AD only; cyan nodes present in HC only; green nodes had group diff. only in 3T; yellow nodes had group diff. only in 7T. The right side of the image denotes the left side of the brain.

4 Discussion

In this paper we used a unique dataset, comparing rich clubs recovered from the same groups of subjects scanned at both 3T and 7T. As the rich club is a relatively new metric in brain connectivity analyses, it is important to know how much measures

vary across key scan parameters. In a prior paper studying this same dataset [4], the 7T protocol had higher SNR than the 3T protocol, as expected from MR theory, but this did not affect the estimates of FA (fractional anisotropy). We ran binary graph theory analyses (not weighted), so some of the more subtle differences between protocols may be washed out. We did not have the space here to consider weighted rich club analyses, but will do so in the future.

One might expect the rich club to contain more nodes at higher field, based on the presumably more accurate and complete recovery of connections. The more extensive rich club seen in the 3T connectome may be due to the higher noise level in this dataset compared to the 7T connectome, which increases the likelihood of false positive fibers. In our group-averaged networks, we did threshold the connectivity matrices to include only those connections found in at least 75% of the subject pool, which should decrease the number of false positives. If specific areas of the brain, such as subcortical structures, are particularly vulnerable to false positives with the 3T protocol, consistent tractography errors may even be made across subjects that are able to survive this thresholding. A weighted analysis might be more sensitive to this, if the false positive connections are weak. We intend to pursue these analyses.

Comparing networks of analogous k -levels is intuitive, as the rich club is defined by statistically high degree nodes. Even so, an analysis of networks thresholded to contain the same *number* of nodes (retaining those with highest degree) is complementary, as it can reveal the true direction of associations masked by differences in degree. When we compared $\phi(k)$ between connectomes, keeping the N_{node} constant (or closer than it would be in a k -level analysis), we found significant differences in $\phi(k)$, across a range of nodal degree thresholds, k , and N_{nodes} . Across these significant ranges, $\phi(k)$ was higher in the 3T connectome than the 7T connectome. Higher $\phi(k)$ indicates a greater density of connections between rich club nodes. This could also be due to differences in signal to noise as discussed above. The 7T protocol revealed a more ‘trimmed down’ rich club network. We started out with a binarized analysis, but a weighted analysis may reveal a very different rich club, as significant increases have been found in the density of subcortical connections in the 7T protocol [4]. Other parcellations will obviously yield different results.

In our elderly dataset, we compared the rich clubs of AD and HC subjects at both 3T and 7T to see how field strength might affect group comparisons. Again, the 3T rich clubs included more nodes than the 7T rich clubs, which led to 12 nodes showing group differences in the 3T matrices that no longer showed group differences at 7T. This could be due to increased noise in the 3T data, or decreased resolution for subcortical structures, or increased susceptibility artifacts in the 7T data. These are only preliminary data, but have important implications for future work using rich club measures to investigate the effects of neurological disorders, especially if rich club is ever to be used as a biomarker of disease.

5 Conclusion

Here we compared the rich club coefficient ($\phi(k)$) and anatomical network organization at 3T and 7T in a group of 23 subjects scanned with both protocols. $\phi(k)$ did

not depend on field strength when compared at analogous k -levels, but it did differ when the N_{node} was kept constant. The 3T connectivity matrices had a higher average degree than did the 7T matrices, leading to our comparing $\phi(k)$ on networks with the same N_{node} , as well as on a k -level. When comparing rich clubs at an analogous k -level, we found a number of differences in which nodes were included in the rich club between protocols. The 3T connectome had a far more extensive rich club than the 7T connectome. When we examined our elderly AD and HC subjects, we similarly found differences only in which nodes were included in the rich club. These preliminary results need further analysis, however, for rich club measures to be reliable biomarkers. As the rich club coefficient is a new metric intended to represent a crucial contributor to network efficiency, we believe these results are important for understanding some of the fundamental factors that may affect rich club calculations.

References

1. Colizza, V. et al. (2006). Detecting rich-club ordering in complex networks. **Nat Phys**, 2, 110-115.
2. Van den Heuvel, M. & Sporns, O. (2011). Rich-club organization of the human connectome. **J Neuroscience**, 31(44), 15775-15786.
3. Dennis, E. L. et al. (2013). Development of the “Rich Club” in Brain Networks from 438 Adolescents and Adults Aged 12 To 30. **IEEE ISBI**, 620-623.
4. Zhan, L. et al. (2013). Magnetic resonance field strength effects on diffusion measures and brain connectivity networks. **Brain Connectivity**, 3(1), 72-86.
5. Stanisiz, G. J. et al. (2005). T1, T2 relaxation and magnetization transfer in tissue at 3T. **Magn Reson Med**, 54, 507–512.
6. Yacoub, E. et al. (2003). Spin-echo fMRI in humans using high spatial resolutions and high magnetic fields. **Magn Reson Med**, 49, 655–664.
7. Gallichan, D. et al. (2010). Addressing a systematic vibration artifact in diffusion-weighted MRI. **Hum Brain Mapp**, 31, 193–202.
8. Smith, S. M. et al. (2004). Advances in functional and structural MR image analysis and implementation as FSL. **NeuroImage**, 23, 208–219.
9. Woolrich, M. W. et al. (2009). Bayesian analysis of neuroimaging data in FSL. **NeuroImage**, 45, S173–S186.
10. Wang, R. et al. (2007). Diffusion Toolkit: A Software Package for Diffusion Imaging Data Processing and Tractography. **Proc Intl Soc Magn Reson Med**, 15.
11. Basser, P. J. et al. (2000). In vivo fiber tractography using DT-MRI data. **Magn Reson Med**, 44, 625–632.
12. Duarte-Carvajalino, J. M. et al. (2012) Hierarchical topological network analysis of anatomical human brain connectivity and differences related to sex and kinship. **NeuroImage**, 59 (4), 3784-3804.
13. Desikan, R. S. et al. (2006). An automated labeling system for subdividing the human cerebral cortex on MRI scans into gyral based regions of interest. **NeuroImage**, 31, 968–980.
14. Morgan, V. L. et al. (2009). Integrating functional and diffusion magnetic resonance imaging for analysis of structure-function relationship in the human language network. **PLoS One**, 4, e6660.
15. Rubinov, M. & Sporns, O. (2010). Complex network measures of brain connectivity: uses and interpretations. **NeuroImage**, 52, 1059-1069.
16. Benjamini, Y & Hochberg, Y. (1995). Controlling the false discovery rate: a practical and powerful approach to multiple testing. **J Roy Stat Soc B**, 57(1), 289-300.